A Land-Surface Process/Radiobrightness Model with Coupled Heat and Moisture Transport for Freezing Soils

Yuei-An Liou, *Member, IEEE,* and A. W. England, *Fellow, IEEE*

Abstract— **Phase change of water is an important sink and source of energy and moisture within soils as well as a significant influence upon soil temperature and moisture profiles. These profiles play a crucial role in governing energy and moisture fluxes between bare soils and the atmosphere. They also codetermine radiobrightness, so that the difference between modeled and observed radiobrightness becomes a measure of error in a model's estimate of temperature or moisture.**

In this paper, we present a physically based, coupled-heat and moisture-transport, one-dimensional hydrology/radiobrightness (1 dH/R) model for bare, freezing and thawing, moist soils that are subject to insolation, radiant heating and cooling, and sensible and latent heat exchanges with the atmosphere. We use this model to examine thermal, hydrologic, and Special Sensor Microwave/Imager (SSM/I) radiobrightness signatures for a three-month, dry-down simulation in the fall and winter of the northern United States Great Plains as part of an investigation of the effects of coupling heat and moisture transport. Given a typical initial moisture content of 38%, we find that coupled transport results in a reduction of ice in the surface soil by 21%. The range of diurnal variations in temperature are not significantly affected by coupled transport. Diurnal variations in the 19-GHz, H-polarized radiobrightness can be greater in the coupled transport case by 37 K. Total diurnal variation can exceed 57 K during periods of diurnal freezing and thawing.

I. Introduction

LAND-SURFACE processes are strongly coupled to the dynamics and thermodynamics of the atmosphere through the exchange of moisture, energy, and momentum [1], [2]. Surface temperature and moisture content/state are key parameters in partitioning land-atmosphere energy exchanges into radiant, sensible, and latent heat processes, and they also govern the thermal and microwave brightness if soils are bare or sparsely vegetated. For example, satellite radiometry has been used to infer surface temperature [3] and moisture [4], [5] and to estimate surface heat fluxes [6], [7].

Land-surface process (LSP) models exchange moisture, energy, and momentum with atmospheric models to simulate the land-atmosphere interactions. The LSP models use the parameter soil wetness or soil water to denote the moisture in soil and vegetation that is available to the atmosphere through evaporation or transpiration. Errors in the magnitude of this parameter can cascade through consequent errors in the moisture and energy fluxes to produce significant errors in the atmospheric models [1].

We would like to use radiobrightness's sensitivity to surface moisture to obtain an estimate of the moisture content of surface soils and to relate this soil moisture to an LSP model's soil wetness; that is, to assimilate radiobrightness to improve the LSP estimate of soil wetness. This is not easily done. Current LSP models achieve computational efficiency by employing a greatly simplified, or parameterized, cartoon of physical processes, with the result that soil wetness may not be a true physical quantity that is measurable. Even if it is, current LSP models do not relate near-surface moisture to soil wetness.

A one-dimensional hydrology (1 dH) model can be substituted for an LSP model at the cost of computational efficiency. The stored water parameter in the hydrology model is the functional equivalent of soil wetness, but stored water is a measurable quantity. The hydrology model provides the linkage between near-surface soil moisture and stored water.

Mahfouf [8] used a 1 dH model to estimate stored water from the history of screen-level temperature and humidity. Bouttier *et al.* [9], using a sequential assimilation scheme, substituted their weather driven 1 dH model for the LSP component of a mesoscale model [10]. Similarly, it should be possible to improve, retrospectively, an estimate of stored water by forcing a 1 dH model with data from a model atmosphere and refining the estimate through assimilation of radiobrightness.

We designate the combination of a 1 dH model and a radiobrightness model as our 1 dH/R model. Our first 1 dH/R model with coupled heat and moisture transport was for bare, unfrozen soil [11]. Through this model, we demonstrated that water movement in unfrozen soils strongly influences radiobrightness.

Freezing soils present a very different problem (e.g., [12]). Modeling heat and moisture transfer in partially frozen soils differs from the unfrozen case in the following several ways:

1) liquid water and ice coexist over a wide range of temperatures below the freezing depression point (FDP) [13], [14];
2) liquid water content becomes the iterative solution of highly nonlinear, coupled temperature-suction and water-retention equations;

Manuscript received July 1, 1996; revised April 28, 1997. This work was supported by NASA Hydrology Program Grant NAGW-3430 and by NSC Grant NSC 86-2111-M-008-035-T.

Y.-A. Lou is with the Center for Space and Remote Sensing Research, National Central University, Chung-Li, Taiwan, R.O.C. (e-mail: yueian@csrsr.ncu.edu.tw).

A. W. England is with the Departments of Electrical Engineering and Computer Science and Atmospheric, Oceanic, and Space Sciences, The University of Michigan, Ann Arbor, MI 48109-2122 USA (e-mail: england@eecs.umich.edu).

Publisher Item Identifier S 0196-2892(98)00739-6.

0196–2892/98$10.00 © 1998 IEEE

3) temperature-moisture content curves for repeatedly freezing and thawing soils exhibit hysteresis [15], [16]; and
4) ice lensing and frost heaving occur as liquid water is drawn to the freezing front [17], [18].

One or more of these processes are frequently ignored to make the problem more tractable. For example, Harlan [19] ignored hysteresis, frost heaving, and the effects of the vapor phase on both heat and moisture transport in his study of coupled heat and moisture transport in partially frozen, unsaturated soils. The Harlan model was adopted by Taylor and Luthin [20] and Pikul *et al.* [21]. Later, Flerchinger and Saxton included the effects of the vapor phase on heat and moisture transport [22], but used the simple water-retention model of Brooks and Corey [23].

Modern hydrologic models for porous, unsaturated soils are based upon the theory of heat and moisture transport by Philip and de Vries [24] and [25]. The Philip and de Vries theory includes heat and moisture transport, due to temperature gradients, liquid water concentration gradients, pressure gradients, and gravity.

As ice content increases in freezing soils, intuition would suggest that the transport coefficients should decrease. Konrad and Duquennoi [18] recently proposed transport coefficients that are proportional to a power of the ratio between liquid water content and void space. Below FDP, liquid water is essentially a function of temperature alone [13]. Unless void space is interpreted as pore space less ice volume, allowing temperature to determine liquid water content means that the Konrad and Duquennoi transport coefficients are also determined, even though ice content would vary with total water content. We avoid the ambiguity by reverting to the older theory of Taylor and Luthin [20], where transport coefficients unambiguously decrease with increasing ice content at a fixed temperature.

Our objective is to examine the influence of water transport upon soil temperature, moisture, and radiobrightness of bare soil during a 90-day dry-down simulation in the fall and winter at northern latitudes. For these simulations, we have intentionally ignored only the hysteresis in the freeze/thaw cycle.

II. Hydrology Model

The principal differences between our 1 dH model for nonfreezing soils and that for freezing soils are the additional mass and energy terms associated with ice in the conservation equations, the ice-dependent reduction factors for the transport coefficients, a temperature-suction relation that is used iteratively to estimate liquid water content, and a modified numerical scheme.

A. Governing Equations and Associated Terms

Ice represents a lower energy state than liquid water, so that the moisture and heat contents per unit volume (see [11, Eqs. (1) and (2)]) become

$$X_m = \rho_l\theta_l + \rho_v\theta_a + \rho_i\theta_i \tag{1}$$

$$X_h = (C_d + c_l\rho_l\theta_l + c_p\rho_v\theta_a + c_i\rho_i\theta_i)(T - T_0) + L_{v_0}\rho_v\theta_a - L_{f_0}\rho_i\theta_i - \rho_l\int_0^{\theta_l} W\,d\theta \tag{2}$$

where

X_m	total mass of moisture per unit volume, kg/m^3;
X_h	total heat content per unit volume, J/m^3;
ρ_l	density of liquid water, kg/m^3;
θ_l	volumetric liquid water content, m^3/m^3;
ρ_v	density of water vapor, kg/m^3;
θ_a	volumetric air content, m^3/m^3;
ρ_i	density of ice, kg/m^3;
θ_i	volumetric ice content, m^3/m^3;
C_d	volumetric heat capacity of a dry porous medium, J/m^3-K;
c_l	specific heat of liquid water at constant pressure, J/kg-K;
c_p	specific heat of water vapor at constant pressure, J/kg-K;
c_i	specific heat of ice at constant pressure, J/kg-K;
T	temperature, K;
T_0	reference temperature, K;
L_{v_0}	latent heat of vaporization at the reference temperature, J/kg;
L_{f_0}	latent heat of fusion at the reference temperature, J/kg;
W	differential heat of wetting [25], J/kg.

The governing equations of heat and moisture transport become

$$\left[1 + \frac{(S-\theta_l-\theta_i)\rho_0}{\rho_l}\frac{\partial h_r}{\partial\theta_l} - \frac{\rho_v}{\rho_l}\right]\frac{\partial\theta_l}{\partial t} + \frac{(S-\theta_l-\theta_i)}{\rho_l}\left(h_r\frac{\partial\rho_0}{\partial T} + \rho_0\frac{\partial h_r}{\partial T}\right)\frac{\partial T}{\partial t} + (\rho_i - \rho_v)\frac{\partial\theta_i}{\partial t} = \nabla\cdot\left(D_T\nabla T + D_\theta\nabla\theta_l + K\hat{k}\right) \tag{3}$$

$$\left[L_v(S-\theta_l-\theta_i)\rho_0\frac{\partial h_r}{\partial\theta_l} - L_v\rho_v - \rho_l W\right]\frac{\partial\theta_l}{\partial t} + \left[C + L_v(S-\theta_l-\theta_i)\left(h_r\frac{\partial\rho_0}{\partial T} + \rho_0\frac{\partial h_r}{\partial T}\right)\right]\frac{\partial T}{\partial t} + (L_f\rho_i - L_v\rho_v)\frac{\partial\theta_i}{\partial t} = \nabla\cdot[(\lambda_* + L_v\rho_l D_{T_v})\nabla T] + L_v\rho_l\nabla\cdot(D_{\theta_l}\nabla\theta_l) + \rho_l\left[(c_p D_{\theta_v} + c_l D_{\theta_l})\nabla\theta_l + (c_p D_{T_v} + c_l D_{T_l})\nabla T + c_p K\hat{k}\right]\cdot\nabla T \tag{4}$$

where

S	porosity;
ρ_0	density of saturated water vapor, kg/m^3;
h_r	relative humidity;
$D_T = D_{T_l} + D_{T_v}$	thermal moisture diffusivity, m^2/K-s;
$D_\theta = D_{\theta_l} + D_{\theta_v}$	isothermal moisture diffusivity, m^2/s;
D_{T_l}	thermal liquid diffusivity;
D_{T_v}	thermal vapor diffusivity;
D_{θ_l}	isothermal liquid diffusivity;

D_{θ_v} isothermal vapor diffusivity;
K hydraulic conductivity, m/s;
$\hat{k}$ vertical unit vector;
L_v $L_{v_0} + (c_l + c_p)(T - T_0)$;
L_f $L_{f_0} - (c_l - c_i)(T - T_0)$;
λ_* thermal conductivity of a moist porous medium, J/m-K-s.

The transport coefficients of heat and moisture for the partially frozen soil are obtained by dividing their corresponding values for an unfrozen soil with the same liquid water content by a reduction factor, i.e.,

$$D = D_u / I \tag{5}$$

where D represents $D_T, D_\theta, D_{T_l}, D_{T_v}, D_{\theta_l}, D_{\theta_v}$, or K, and the subscript u denotes an unfrozen value. The reduction factor I is given by [20] as

$$I = 10^{10\theta_i}. \tag{6}$$

B. Temperature-Suction Relation

The temperature-suction relation is [13]

$$\Psi = \frac{L_f(T) \cdot T_{\text{fpd}}}{Tg} \tag{7}$$

where

Ψ suction (matric head) in meters;
$L_f(T)$ latent heat of fusion of water at temperature T, J/kg;
T_{fpd} freezing point depression, K;
g acceleration due to gravity, m/s^2.

The temperature-suction relation is combined with the Rossi and Nimmo [28] model of water retention to iteratively determine the liquid water content below the FDP.

C. Numerical Scheme

Differences between the nonfreezing and freezing soil models that affect the numerical scheme are the following: 1) moisture state may change from one time step to the next, 2) unfrozen water content is sensitive to temperature, and, 3) the two governing equations, (1) and (2), are independent above FDP, but become dependent at temperatures below FDP.

Fig. 1 shows the flowchart of the 1 dH model algorithm. We initialize temperature, moisture content, and moisture state profiles by using results from an annual thermal model [26]. Convergence in the frozen case often requires multiple iterations for each layer at each time step.

For a two-dimensional (2-D) Newton–Raphson problem (unfrozen soil), the criteria for convergence include 1) the change in temperature between iterations must be less than 0.01 K and 2) the change in liquid water content between iterations must be less than 0.01%. However, 1) is the only convergence criterion for a one-dimensional (1-D) Newton–Raphson problem (frozen soil).

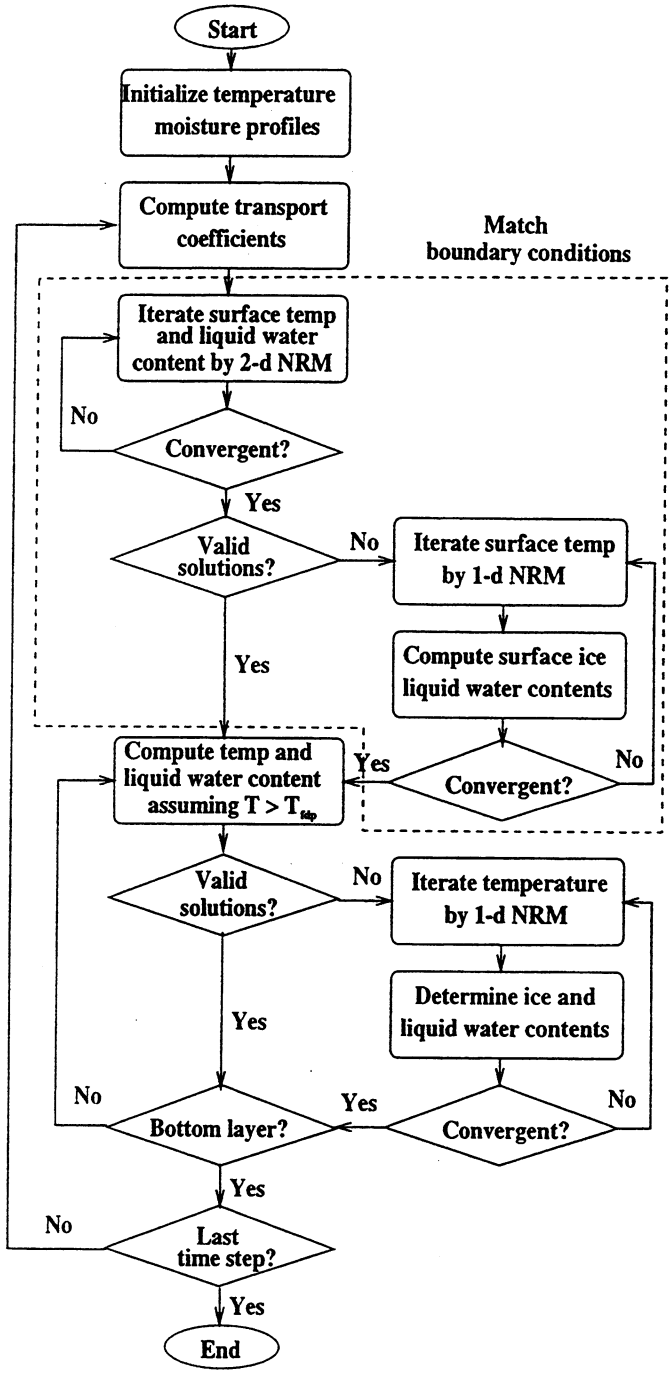

Fig. 1. Flowchart of the 1 dH model algorithm for freezing soils. "NRM" denotes the Newton–Raphson method [27].

D. Results

The model was run for a 90-day period for both water transport and no water transport cases in soil at a northern latitude of 43.5° in fall and early winter (10/15-01/12). These times were chosen to span the transition between diurnal periods without freezing and diurnal periods without significant thawing. Initial temperature and moisture profiles are from an annual thermal model [26] in which soil moisture was a uniform 38% at all depths for the year. The heat flux at soil depths below the influence of the diurnal cycle was assigned to be that observed in the annual model.

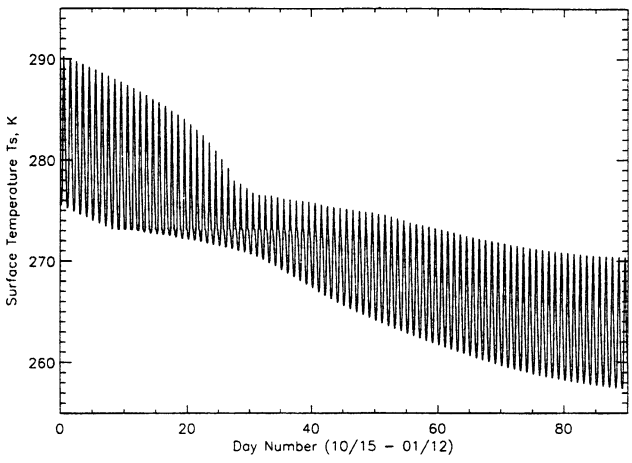

(a)

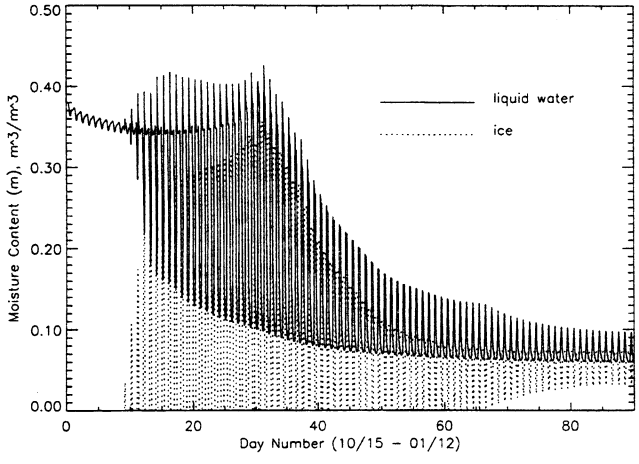

(b)

Fig. 2. (a) Temperature and (b) liquid water and ice contents at the surface for the water transport case.

Fig. 2 shows the temperature, liquid water content, and ice content of the surface layer as a function of time for the water transport case. The 90-day simulation period can be divided into three subperiods based upon surface wetness.

A) *Day 1 to day 8: The first drying period.* Both surface temperature and liquid water content exhibit regular diurnal oscillations with decreasing means.

B) *Day 9 to day 30: The fluctuating period.* Nighttime temperatures begin to drop below the FDP. Between day 9 and day 65, the diurnal variation in temperature is suppressed by the diurnal freezing and thawing of surface moisture. This fluctuating period is characterized by dramatic daytime increases and nighttime decreases in surface liquid water. Fig. 3 shows the temperature, liquid water content, and ice-content profiles over a typical diurnal cycle for the fluctuating period. We observe the following.

1) Freezing occurs toward the end of the previous night.
2) Updrawing of excess water from the soil layers below the freezing front significantly increases the total moisture content of the top soil layer.
3) As surface cooling moves the freezing front downward, more near-surface soil layers reach high moisture contents.

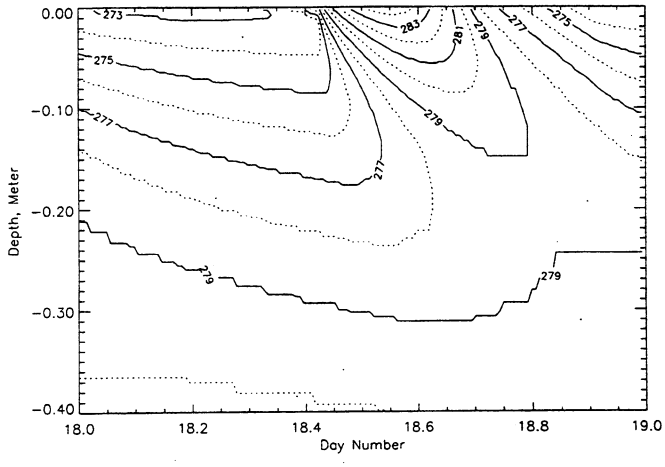

(a)

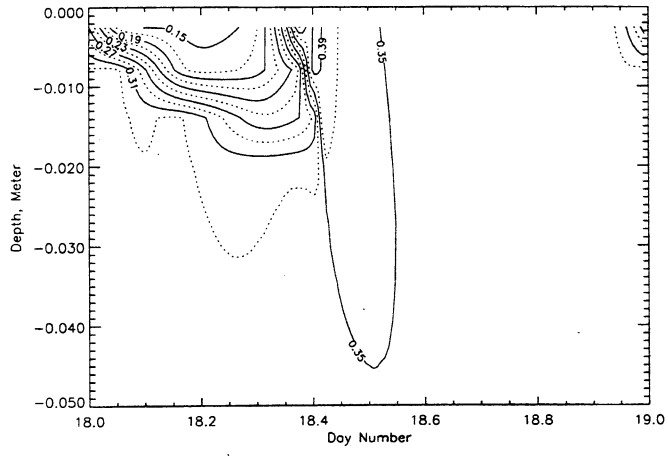

(b)

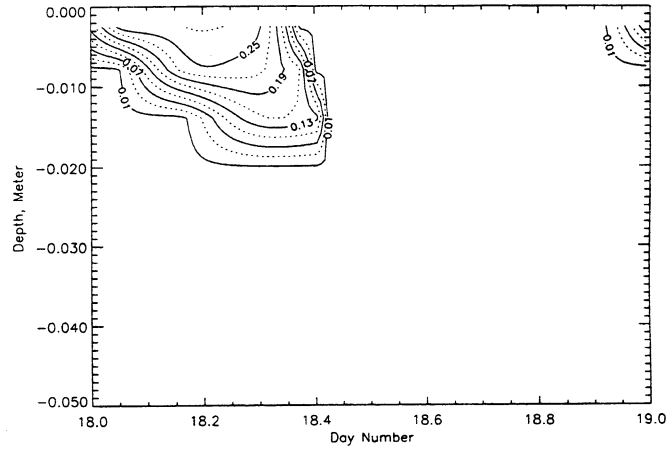

(c)

Fig. 3. (a) Temperature, (b) liquid water content, and (c) ice-content profiles over a diurnal cycle on day 19. Sunrise occurs at 7:10 am, with a peak insolation of 360 W/m^2 at 12:10 pm. The sun sets at 5:20 pm. Note the change in vertical scales from 40 cm in (a) to 5 cm in (b) and (c).

4) A large portion of the solar heating immediately after sunrise is spent melting the ice within the top soil layer, then the second layer, then the third layer, etc., so that the quantity of liquid water at the surface increases rapidly.

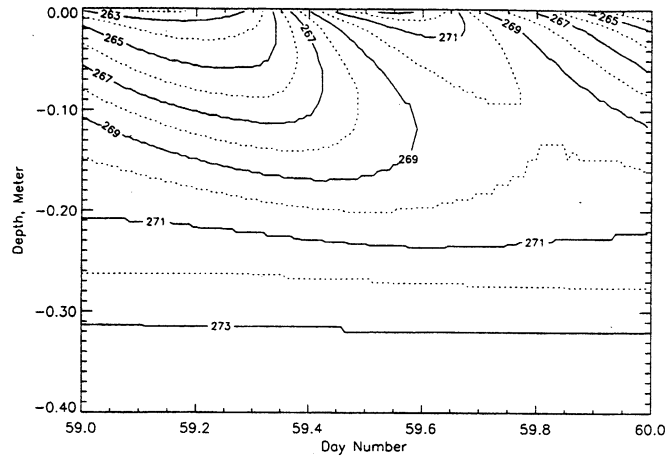

(a)

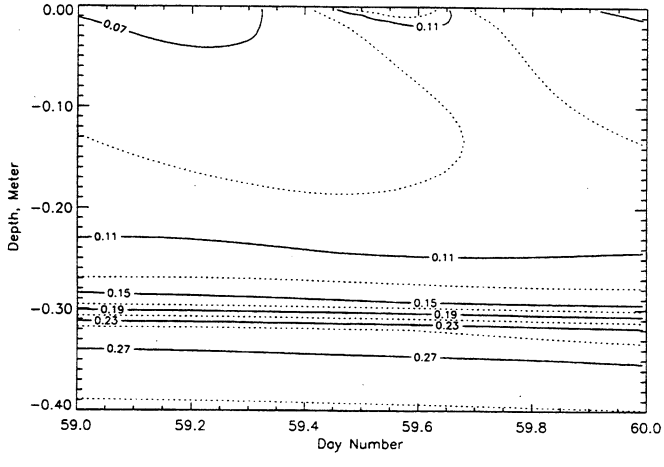

(b)

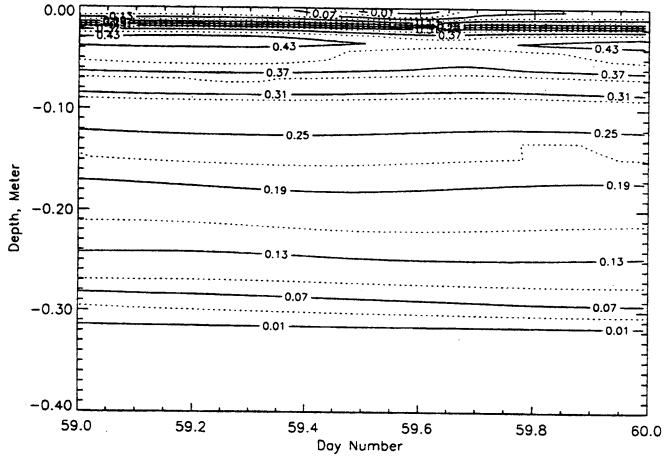

(c)

Fig. 4. (a) Temperature, (b) liquid water content, and (c) ice-content profiles over a diurnal cycle on day 60. Sunrise occurs at 7:20 am, with a peak insolation of 290 W/m^2 at 12:10 pm. The sun sets at 5 pm.

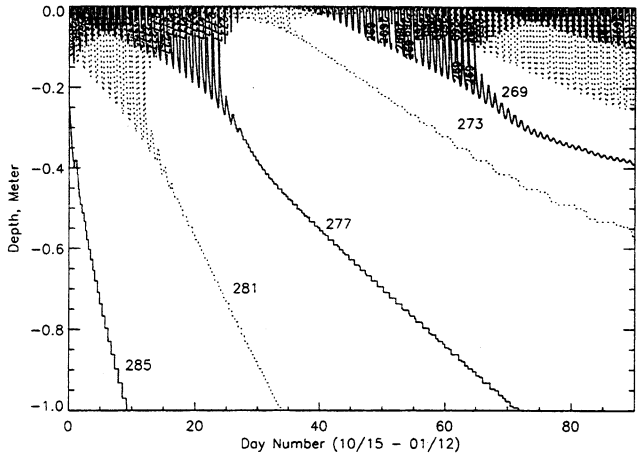

(a)

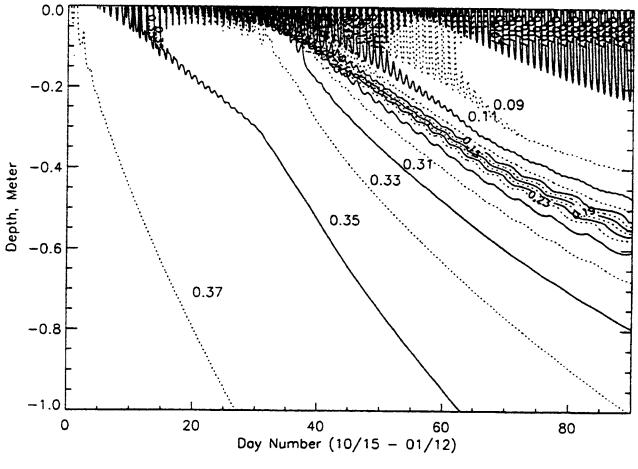

(b)

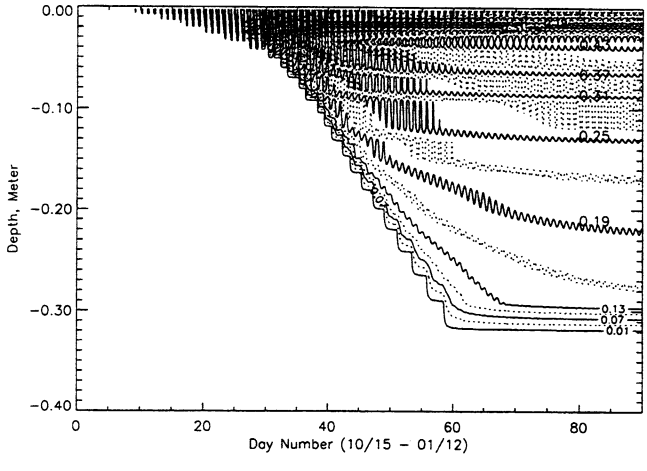

(c)

Fig. 5. (a) Temperature, (b) liquid water content, and (c) ice-content profiles for the water transport case. Note that the depth scale of (c) differs from that of (a) and (b).

5) Ice within the top soil layer completely melts, causing the liquid water content to surge to about 40% in mid-morning. After that maximum, moisture is removed by downward moisture transport and by upward evaporation [see Fig. 7(a) and (b)]. A similar process occurs at the interfaces between deeper soil layers to cause additional surges in surface liquid water content, but their significance is diminished. The discrete pattern of moisture surges is an artifact of layers of finite thickness. If layers were to become infinitely thin, the surges would smooth to a single diurnal surge.

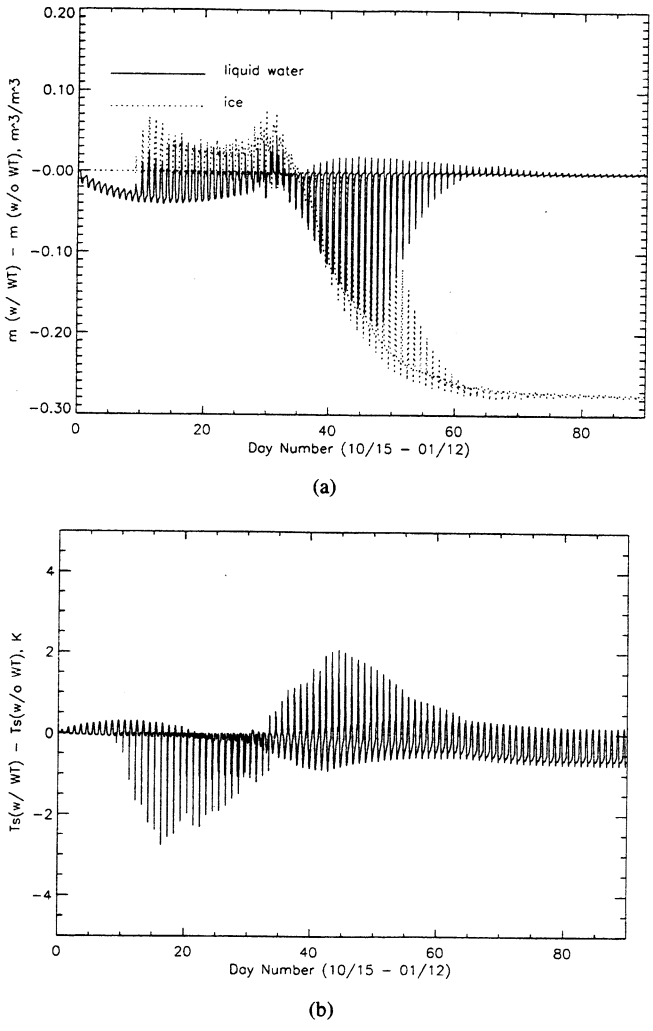

Fig. 6. Differences in (a) liquid and ice contents and in (b) temperature at the surface between the water transport and no water transport cases.

C) *Day 31 to day 90: The second drying period.* The diurnal variation in temperature over this 60-day period increases with increasing day number from 6 K on day 31 to 13 K on the last day [Fig. 2(a)]. The increase follows decreases in surficial liquid water and ice contents as the freezing front moves downward [also see Fig. 5(b)]. The thickening of the frozen soil zone as the freezing front moves downward increasingly restricts the resupply of moisture to the surface layer from deeper soil layers. From day 31 to day 50, the total water content of the top layer of soil decreases to about 25%, while, from day 50 to day 90, the decrease is only another 4%. Beginning with day 67, ice in the top soil layer never melts completely during daytime. After this date, there is little latent heat transfer between the air and the land. The temperature, liquid water content, and ice-content profiles for day 60 are shown in Fig. 4. For temperatures below the FDP, liquid water content is a function of temperature so that Fig. 4(b) is highly correlated with Fig. 4(a). Fig. 4(c) shows that ice content generally decreases with increasing depth except near the surface where soil is subject to diurnal cooling and heating.

Temperature profiles for the 90-day water transport case are shown in Fig. 5(a). The near-surface, downward, lobe-shaped isotherms are a response of soil to diurnal heating and cooling at the land-air interface. Their penetration depths strongly correlate with the strength of diurnal weather forcing and inversely with the thermal inertia of the soil. The shallowest penetration, less than 6 cm, corresponds to the 273-K isotherm around day 30 when soil freezing and thawing are most extensive. This phase change of water dominates other factors in governing the thermal inertia of the soil. Similarly, the 273-K isotherm penetrates to deeper soils more slowly than do the 281- and 285-K isotherms. The profiles of temperature [Fig. 5(a)] and of liquid water content [Fig. 5 (b)] exhibit the correlation shown in Fig. 4(a) and (b) for one day.

Profiles of ice content for the water transport case are shown in Fig. 5(c). Frozen soil thickness increases until day 60. After day 60, there is insufficient cooling of the soil column for the freezing front to progress further downward. By day 31, a permanent frozen soil layer forms at about 3-cm depth. By day 43, the highest ice content (43%) appears at about 4-cm depth. By the end of the 90-day simulation, this region of high ice content is 1-cm thick and lies at a depth of 3.5 cm. Away from the ice maximum, ice content decreases monotonically with both increasing and decreasing depths.

Differences in surface liquid water and ice contents between the water transport and no water transport cases are shown in Fig. 6(a). The maximum difference in liquid water content over the 90-day simulation is 19% on day 47. The maximum difference in ice content is 27% during the last 30 days of the simulation. As expected in a dry-down simulation, surface moisture content (liquid water plus ice contents) for the water transport case is generally lower than that of the no water transport case. Exceptions occur when the freezing front is near the surface, so that the surface layer can extract moisture from the soil layers below. This phenomenon can be seen during the nighttime between day 10 and day 33.

Total moisture content within the depth range of diurnal thermal pulses is lower for the water transport case than for the no water transport case. Consequently, the water transport case exhibits warmer surface temperatures during daytime and cooler surface temperatures during nighttime [Fig. 6(b)]. Maximum differences near day 45 coincide with the period of maximum difference in liquid water content.

Fig. 7 offers detailed views of diurnal variations in surface temperature and moisture content/state on days 19, 44, and 60 for both water transport and no water transport cases. Freezing and thawing are the dominant processes—particularly on days 19 and 44.

III. Radiobrightness Model

Nearly daily radiometric observations for higher latitudes from the Defense Meteorological Satellite's SSM/I [29] have been available since 1987. Radiobrightness is sensitive to moisture in bare or sparsely vegetated soils through the Debye relaxation process of liquid water. Here, we examine the radiobrightness of freezing and thawing bare soils at the SSM/I frequencies.

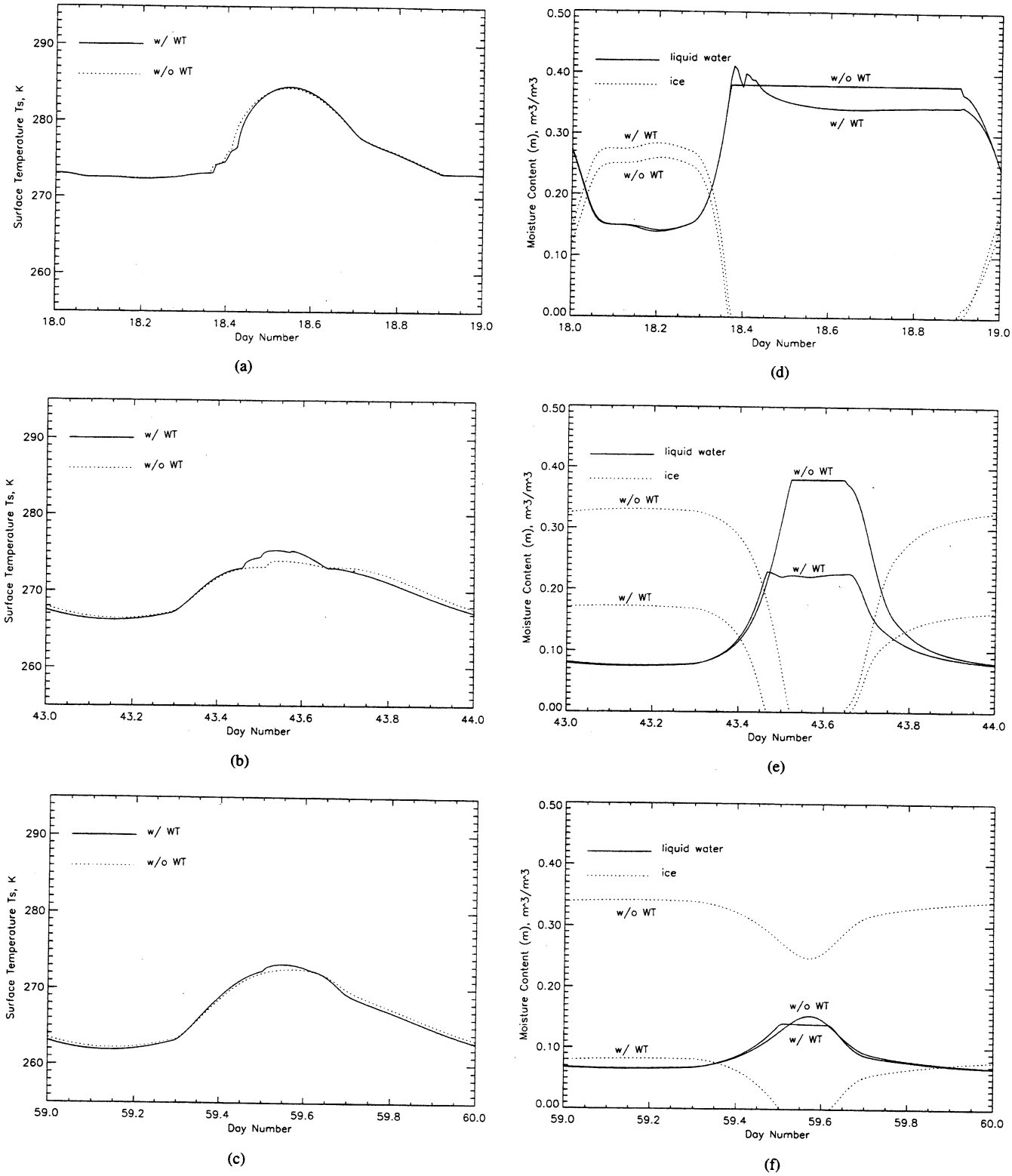

Fig. 7. Surface temperatures on (a) day 19, (b) day 44, and (c) day 60. Liquid water and ice contents on (d) day 19, (e) day 44, and (f) day 60.

The SSM/I radiobrightnesses of bare, wet soil are estimated with a microwave emission model for a quasispecular, homogeneous soil

$$T_b(t) = e \cdot T_{\text{eff}}(t) \tag{8}$$

where e is a Fresnel reflectivity-based emissivity and $T_{\text{eff}}(t)$ is an effective surface temperature [11], [26]. This approximation is appropriate for bare or sparsely vegetated soil at 19 GHz, but increasingly less appropriate at 37 and 85 GHz, where soil surfaces are increasingly rough at the scale of wavelength.

$$T_{\text{eff}}(t) = T_g(0,t) + \frac{1}{\kappa_e \sec\theta_t} \cdot \left(\frac{\partial T_g(z,t)}{\partial z}\right)_{z=0} \tag{9}$$

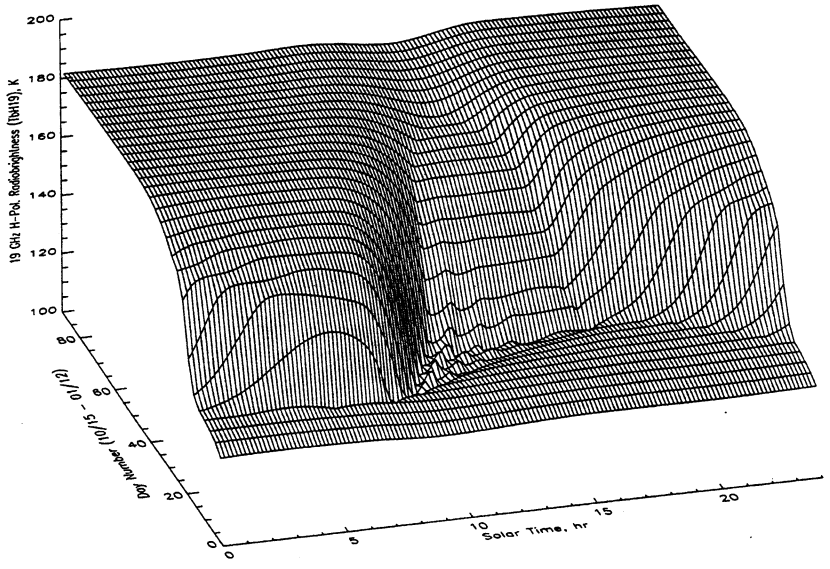

(a)

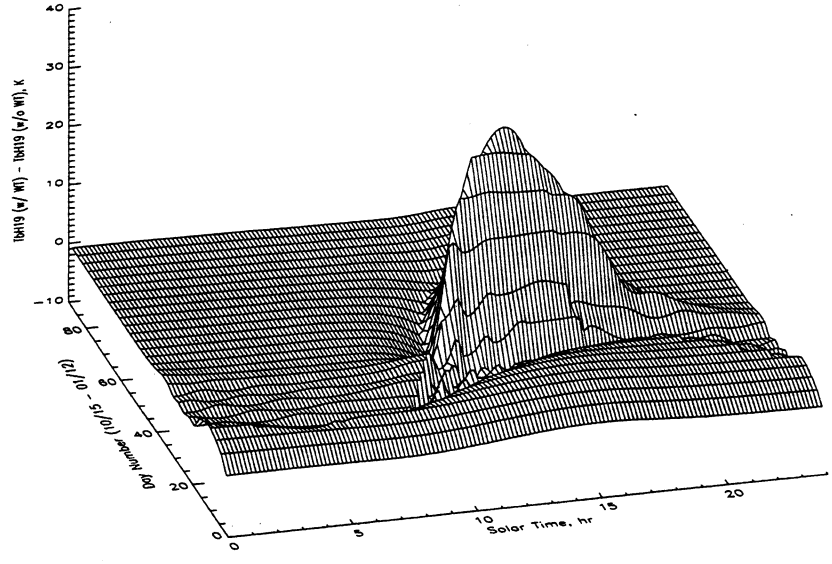

(b)

Fig. 8. (a) H-polarized, 19-GHz radiobrightness for the water transport case. (b) Differences in H-polarized, 19-GHz radiobrightness between the water transport and no water transport cases.

where κ_e is extinction of the soil, θ_t is a transmission angle, and T_g is the ground temperature. As shown in [26], the diurnal extremes of the first-order terms are approximately ± 0.3 K at 19 GHz for 17% moist soil, and they decrease with increasing frequency and water content.

The 90-day, H-polarized, 19-GHz radiobrightness for the water transport case is shown in Fig. 8(a). A significant contrast in radiobrightness, more than 50 K between the first 10-day and the last 30-day periods, reflects the dominant influence of liquid water on radiobrightness. The difference in liquid water content between the two periods is 20%. Similarly, differences in radiobrightness between daytime and nighttime are highly correlated with variations in the liquid water content over a diurnal cycle. The maximum diurnal variation in radiobrightness of 57 K is seen near day 30 when the surface liquid water content changes by 32% over a diurnal cycle [see Fig. 2(b)].

Differences in H-polarized, 19-GHz radiobrightness between the water transport and no water transport cases are shown in Fig. 8(b). The maximum difference of 37 K appears near day 48 when the difference in surface liquid water content between the two cases is the largest [Fig. 6(a)].

The maximum and minimum differences in 19-GHz, H-polarized radiobrightness between water transport and no water transport cases at 2 am, 6 am, 2 pm, and 6 pm are shown in Table I. Clearly, vertical water transport is an important influence upon the radiobrightness of bare soil. The 37- and 85-GHz differences are smaller.

Note that the effects of scatter darkening on the SSM/I radiobrightnesses are not accounted for in (8). Scatter darkening within frozen soils results from the fact that freezing reduces the imaginary part of the soil dielectric constant [30] so that volume scattering becomes relatively significant at higher frequencies.

TABLE I
MAXIMUM AND MINIMUM OF T_b (WATER TRANSPORT)—T_b (NO WATER TRANSPORT) FOR 19-GHz HORIZONTAL POLARIZATION

Differences, K	maximum	minimum
2 a.m.	3.8	-0.4
6 a.m.	3.5	-3.4
2 p.m.	31.8	-2.4
6 p.m.	12.7	-2.6

IV. CONCLUSION

Water transport in bare or sparsely vegetated soils has a significant influence upon radiobrightness. The influence is particularly noticeable during periods of diurnal freezing and thawing.

The three significant hydrologic features of the 90-day dry down during fall for bare soils in northern latitudes are the following:

1) the decrease in the total moisture content at the surface is about 25%;
2) there can be brief surges in daytime surface liquid water during periods of diurnal freezing and thawing; and
3) an ice-rich layer develops at a depth of about 3.5 cm.

The significant radiobrightness feature of the 90-day dry down is the dramatic diurnal variation in radiobrightness as soils freeze and thaw.

This LSP/R model for bare soil will be mixed with an LSP/R model for prairie grassland to model mixed terrains in the northern prairie [31]. The LSP/R model for prairie grassland will be presented in a companion paper [32]. Both models will be validated against our field data from REBEX-1 [12] and REBEX-4 (during the summer of 1996) on the prairie near Sioux Falls, SD.

REFERENCES

[1] P. R. Rowntree and J. R. Bolton, "Simulation of the atmospheric response to soil moisture anomalies over Europe," *Q. J. R. Meteorol. Soc.*, vol. 109, pp. 501–526, 1983.

[2] C. B. Smith, M. N. Lakhtakia, W. J. Capehart, and T. N. Carlson, "Initialization of soil-water content in regional-scale atmospheric prediction models," *Bull. Amer. Meteorol. Soc.*, vol. 75, pp. 585–593, 1994.

[3] M. Sugita and W. Brutsaert, "Comparison of land surface temperatures derived from satellite observations with ground truth during FIFE," *Int. J. Remote Sensing*, vol. 14, pp. 1659–1676, 1993.

[4] B. J. Choudhury and R. E. Golus, "Estimating soil wetness using satellite data," *Int. J. Remote Sensing*, vol. 9, pp. 1251–1257, 1988.

[5] N. U. Ahmed, "Estimating soil moisture from 6.6 GHz dual polarization, and/or satellite derived vegetation index," *Int. J. Remote Sensing*, vol. 16, pp. 687–708, 1995.

[6] W. Brutsaert and M. Sugita, "Regional surface fluxes from satellite-derived surface temperatures (AVHRR) and radiosonde profiles," *Boundary-Layer Meteorol.*, vol. 58, pp. 355–366, 1992.

[7] X. Huang, T. J. Lyons, R. C. G. Smith, J. M. Hacker, and P. Schwerdtfeger, "Estimation of surface energy balance from radiant surface temperature and NOAA AVHRR sensor reflectances over agricultural and native vegetation," *J. Appl. Meteorol.*, vol. 32, pp. 1441–1449, Aug. 1993.

[8] J.-F. Mahfouf, "Analysis of soil moisture from near-surface parameters: A feasibility study," *J. Appl. Meteorol.*, vol. 30, pp. 1534–1547, 1991.

[9] F. Bouttier, J.-F. Mahfouf, and J. Noilhan, "Sequential assimilation of soil moisture from atmospheric low-level parameters. Part I: Sensitivity and calibration studies," *J. Appl. Meteorol.*, vol. 32, pp. 1335–1351, Aug. 1993.

[10] ——, "Sequential assimilation of soil moisture from atmospheric low-level parameters. Part II: Implementation in a mesoscale model," *J. Appl. Meteorol.*, vol. 32, pp. 1352–1364, Aug. 1993.

[11] Y.-A. Liou and A. W. England, "A land surface process/radiobrightness model with coupled heat and moisture transport in soil," *IEEE Trans. Geosci. Remote Sensing*, vol. 36, pp. 273–286, Jan. 1998.

[12] J. F. Galantowicz, "Microwave radiometry of snow-covered grasslands for the estimation of land-atmosphere energy and moisture fluxes," Ph.D. dissertation, Univ. Michigan, Ann Arbor, 1995, p. 196.

[13] P. J. Williams, "Experimental determination of apparent specific heats of frozen soils," *Geotechnique*, vol. 14, pp. 133–142, 1964.

[14] S. C. Brown and D. Payne, "Frost action in clay soils. I. A temperature-step and equilibrate differential scanning calorimeter technique for unfrozen water content determinations below 0°C," *J. Soil Sci.*, vol. 40, pp. 535–546, 1990.

[15] R. W. R. Koopmans and R. D. Miller, "Soil freezing and soil water characteristic curves," in *Proc. Soil Sci. Soc. Amer.*, vol. 30, 1966, pp. 680–685.

[16] K. Horiguchi and R. D. Miller, "Hydraulic conductivity functions of frozen materials," in *Proc. 4th Int. Conf. Permafrost*, Nat. Acad. Sci., Washington, DC, 1983, pp. 289–294.

[17] D. M. Anderson and N. R. Morgenstern, "Physics, chemistry, and mechanics of frozen ground: A review," in *Proc. 2nd Int. Conf. Permafrost*, Nat. Acad. Sci., Washington, DC, 1973, pp. 289–294.

[18] J.-M. Konrad and C. Duquennoi, "A model for water transport and ice lensing in freezing soils," *Water Resour. Res.*, vol. 29, pp. 3109–3124, 1993.

[19] R. L. Harlan, "Analysis of coupled heat-fluid transport in partially frozen soil," *Water Resour. Res.*, vol. 9, pp. 1314–1323, 1973.

[20] G. S. Taylor and J. N. Luthin, "A model for coupled heat and moisture transfer during soil freezing," *Can. Geotech. J.*, vol. 15, pp. 548–555, 1978.

[21] J. L. Pikul, Jr., L. Boersma, and R. W. Rickman, "Temperature and water profiles during diurnal soil freezing and thawing: Field measurements and simulation," *Soil Sci. Soc. Amer. J.*, vol. 53, pp. 3–10, 1989.

[22] G. N. Flerchinger and K. E. Saxton, "Simultaneous heat and water model of a freezing snow-residue-soil system I. Theory and development," *Trans. ASAE*, vol. 32, pp. 565–571, 1989.

[23] R. H. Brooks and A. T. Corey, "Properties of porous media affecting fluid flow," *J. Irrig. Drain. Div. Amer. Soc. Civ. Eng.*, vol. 92, pp. 61–87, 1966.

[24] J. R. Philip and D. A. de Vries, "Moisture movement in porous materials under temperature gradients," *Trans. Amer. Geophys. Union*, vol. 38, pp. 222–232, Apr. 1957.

[25] D. A. de Vries, "Simultaneous transfer of heat and moisture in porous media," *Trans. Amer. Geophys. Union*, vol. 39, pp. 909–916, Oct. 1958.

[26] Y.-A. Liou and A. W. England, "Annual temperature and radiobrightness signatures for bare soils," *IEEE Trans. Geosci. Remote Sensing*, vol. 34, pp. 981–990, July 1996.

[27] W. H. Press, B. P. Flannery, S. A. Teukolsky, and W. T. Vetterling, *Numerical Recipes (FORTRAN).* Cambridge, U.K.: Cambridge Univ. Press, 1989, p. 702.

[28] C. Rossi and J. R. Nimmo, "Modeling of soil water retention from saturation to oven dryness," *Water Resour. Res.*, vol. 30, pp. 701–708, Mar. 1994.

[29] J. Hollinger, R. Lo, G. Poe, R. Savage, and J. Pierce, *Special Sensor Microwave/Imager User's Guide*, Naval Res. Lab., Washington, DC, 1987.

[30] B. W. Zuerndorfer, A. W. England, C. M. Dobson, and F. T. Ulaby, "Mapping freeze/thaw boundaries with SMMR data," *J. Agriculture Forest Meteorol.*, vol. 52, pp. 199–225, 1990.

[31] Y.-A. Liou, E. J. Kim, and A. W. England, "Radiobrightness of prairie soil and grassland during dry-down simulations," *Radio Sci.*, to be published.

[32] Y.-A. Liou, J. F. Galantowicz, and A. W. England, "A land surface process/radiobrightness model with coupled heat and moisture transport for prairie grassland," submitted for publication.

Yuei-An Liou (S'91–M'96), for a photograph and biography, see p. 286 of the January 1998 issue of this TRANSACTIONS.

A. W. England (M'97–SM'89–F'95), for a photograph and biography, see p. 286 of the January 1998 issue of this TRANSACTIONS.